Available online at www.sciencedirect.com
ScienceDirect
Geochimica et Cosmochimica Acta 75 (2011) 2865–2881
Geochimica et Cosmochimica Acta
www.elsevier.com/locate/gca

Mineralogy, geochemistry, and ^{40}Ar–^{39}Ar geochronology of lunar granulitic breccia Northwest Africa 3163 and paired stones: Comparisons with Apollo samples

Jillian A. Hudgins [a], Simon P. Kelley [b], Randy L. Korotev [c], John G. Spray [a,*]

[a] Planetary and Space Science Centre, University of New Brunswick, 2 Bailey Drive, Fredericton, New Brunswick E3B 5A3, Canada
[b] Centre for Earth, Planetary, Space, and Atmospheric Research (CEPSAR), The Open University, Walton Hall, Milton Keynes MK7 6AA, UK
[c] Department of Earth and Planetary Sciences and McDonnell Center for the Space Sciences, Washington University, St. Louis, Missouri, USA

Received 23 April 2010; accepted in revised form 21 February 2011; available online 1 March 2011

Abstract

The lunar meteorites Northwest Africa (NWA) 3163, 4881, and 4483 are paired stones classified as granulitic breccias. At 2.4 kg, these three stones constitute one of the largest known lunar meteorite masses. Here we describe the petrography, mineralogy, and chemistry of NWA 3163, 4881, and 4483, and present ^{40}Ar–^{39}Ar data for two of the meteorites. Two-pyroxene thermometry indicates that the rocks equilibrated at 1050 ± 50 °C, which represents the high-temperature, low-pressure event that generated their characteristic recrystallization textures and reset their Ar systematics. Stepped-heating, in situ infrared laser microprobe ^{40}Ar–^{39}Ar geochronology yields a mean age of 3327 ± 29 Ma for NWA 3163, and a more disturbed release spectrum for NWA 4881. NWA 4881 shows an upward-trending pattern, suggesting that it may have had a ^{40}Ar–^{39}Ar age of >3.0 Ga, but that it was partially reset at ~2.6 Ga. NWA 3163 et al. exhibit shock effects, including maskelynitized plagioclase, shock veins, and melt pockets, which are absent in the Apollo granulitic breccias. Although the Apollo and meteorite samples are texturally similar and have comparable bulk compositions and equilibration temperatures, their trace and siderophile element contents point to distinct parental lithologies derived from different regions of the Moon. Based on mineralogical and geochemical differences between the Apollo and meteorite samples, we conclude that the parent rock(s) of the paired NWA meteorites came from an area outside the Imbrium region and that they underwent high-temperature (granulite event) metamorphism long after the Late Heavy Bombardment.
© 2011 Elsevier Ltd. All rights reserved.

1. INTRODUCTION

To date, 136 stones from 65 different lunar meteorites representing approximately 45 distinct impact cratering events have been discovered on the Earth's surface (Korotev, 2009). These meteorites provide additional information to the directly acquired Apollo and Soviet Luna samples. The meteorites are derived from a broader range of locations, whereas the Apollo samples were acquired from within, or near, what we now know as the geochemically distinct Procellarum KREEP Terrane (PKT). Along with remote sensing data from the Clementine and Lunar Prospector missions, the lunar meteorite inventory has revealed a lunar crust more diverse than was originally inferred from the Apollo and Luna collections alone, with three main terranes being identified: PKT, Feldspathic Highlands (FHT), and South Pole Aitken (Jolliff et al., 2000, 2006; Korotev, 2005, 2009).

Lunar granulitic breccias are metamorphic rocks (Warner et al., 1977; Lindstrom and Lindstrom, 1986; Cushing et al., 1999) formed when impact-melt breccias and clast-bearing impact melts were heated to 1000–1100 °C until they recrystallized, obliterating original textures (Cushing et al., 1999; Korotev and Jolliff, 2001; Hudgins et al., 2008). The diagnostic feature of lunar granulitic breccias is a granoblastic to poikiloblastic matrix.

* Corresponding author. Tel.: +1 506 453 3550.
E-mail address: jgs@unb.ca (J.G. Spray).

0016-7037/$ - see front matter © 2011 Elsevier Ltd. All rights reserved.
doi:10.1016/j.gca.2011.02.035

They contain, on average, 70 vol% plagioclase and are moderately contaminated with meteoritic siderophile elements, suggesting an impact-related origin for the protoliths of these rocks. Granulitic breccias are not common rocks, but have been found in small amounts at all of the Apollo highlands sampling sites as individual rocks and, more commonly, as clasts in breccias and as fragments in the regolith. Of the 65 lunar meteorites, only four are granulitic breccias: Dhofar (Dho) 026 and its paired stones (James et al., 2003; Cohen et al., 2004; Warren et al., 2005), Dho 733 (Foreman et al., 2008), NWA 5744 (Kuehner et al., 2010), and, the focus of this study, paired stones NWA 3163, 4881, and 4483. By comparison, ten are unbrecciated mare basalts.

Here we describe the petrography and mineralogy of NWA 3163, 4881, and 4483 and present ^{40}Ar–^{39}Ar ages for NWA 3163 and 4881. When not referring to the stones individually, we refer to them collectively as "NWA 3163 et al." In terms of texture and age, we compare NWA 3163 et al. to four Apollo granulitic breccia samples that we previously studied: samples 60035, 77017, 78155, and 79215 (Hudgins et al., 2008). We also present bulk compositional data for NWA 3163 et al., Dho 026, and Dho 733, and compare the granulitic breccias with other lunar meteorites and Apollo samples.

2. ANALYTICAL METHODS

We acquired small (<10 g) samples of NWA 3163 and NWA 4881 from private collectors, from which polished thin (25 μm) and thick (2 mm) sections were made at the University of New Brunswick's preparation lab. We had a thin section of NWA 4483 prepared by a commercial laboratory. A doubly-polished thin section of each sample was examined with a Nikon E400 optical microscope using transmitted and reflected light.

Backscattered electron (BSE) and secondary electron (SE) images were obtained using a Hitachi SU-70 field emission scanning electron microscope (FE-SEM). Additional BSE images and quantitative analysis of mineral and lithic clasts were obtained using a JEOL 6400 analytical scanning electron microscope (ASEM) equipped with an EDAX Phoenix X-ray microanalysis system, Sapphire Si (Li) detector, and Genesis microanalysis software. Operating conditions were 15 kV accelerating voltage, 1.5 nA beam current, and 7–14 mm working distance. ZAF corrections were applied to all analyses, which were calibrated using a multi-element standard block (Type 202-52). Counting times were 50 seconds. Normative mineralogies and bulk densities were calculated using CIPW software by Kurt Hollocher (Union College, Schenectady, New York). Pyroxene compositions were determined by electron probe micro-analysis (EPMA) (for thermometry calculations) using a JEOL JXA-733 electron microprobe equipped with four wavelength dispersive spectrometers, operated at an accelerating voltage of 15 kV and a beam current of 15 nA. Minerals were analyzed using a 1 μm spot size.

In situ laser microprobe $^{40}Ar/^{39}Ar$ stepped-heating analysis was performed on whole rock chips separated from thick sections of NWA 3163 and NWA 4881 at the Open University in Milton Keynes (UK), using a CW 1090 nm fiber laser, focused through a Leica petrological microscope with computer-controlled shutter. Chip sample masses were: NWA 3163 25.4 mg; NWA 4881 24.5 mg. A beam splitter was inserted to reduce the laser power by 95%. Heating steps were achieved by increasing the laser power from 0.05 to 1 W and rastering the beam over the surface for ~30 s at each step. Fusion and total de-gassing was achieved at ~2000 °C. Unfortunately, it was not possible to monitor heating temperatures precisely using this apparatus. Blanks were measured after every two steps and a mean of all the blanks was used to calculate the background levels of gases. The correction factors used were $(^{39}Ar/^{37}Ar)_{Ca} = 0.00065$, $(^{36}Ar/^{37}Ar)_{Ca} = 0.000264$, and $(^{40}Ar/^{39}Ar)_K = 0.0085$ based on analyses of Ca and K salts. Typical blank values are $^{40}Ar = 1 \times 10^{-12}$ cc STP, $^{39}Ar = 0.006 \times 10^{-12}$ cc STP, $^{38}Ar = 0.01 \times 10^{-12}$ cc STP, $^{37}Ar = 0.48 \times 10^{-12}$ cc STP, and $^{36}Ar = 0.035 \times 10^{-12}$ cc STP. Results are presented in Appendix A1.

Cosmic Ray Exposure (CRE) ages presented here are calculated based on the spallogenic ^{38}Ar content of the sample after correction for the presence of ^{38}Ar resulting from neutron interactions with chlorine (Eberhardt et al., 1970). It was assumed that the samples had 4π of exposure since all sides of the meteorites would have been exposed to cosmic rays while in space. The CRE ages represent integrated durations of exposure of the rocks at, or very near to, the surface of the Moon and probably reflect processing (burial-exhumation cycles) during recent impact events. The individual ^{38}Ar production rates were calculated based on the composition of the samples using standard production values for Ca, Fe, Ti, and K (Wieler, 2002, and references therein) and these range from 9.46 to 9.85×10^{-9} cm^3 STP/g Ma. CRE ages are given in Appendix A2.

We analyzed Apollo samples 15418 and 67215 by instrumental neutron activation analysis (INAA) at the same time that we analyzed the samples of Hudgins et al. (2008) by techniques discussed in that paper. The lunar meteorites were analyzed by INAA (mainly trace elements) and electron probe microanalysis (EPMA) of fused powders (major elements) as described in Korotev et al. (2009).

3. SAMPLE DESCRIPTIONS

3.1. Hand samples

NWA 3163 is a 1634 g stone that was found in Mauritania or Algeria in 2005 (Connolly et al., 2006), and purchased from a Moroccan dealer in Ouarzazate by G. Hupé. NWA 4881 is a 606 g stone that was found in 2005 and purchased from a dealer in Ouarzazate in 2007 by Stephan Ralew (Connolly et al., 2007). NWA 4483 is a 208 g stone that was purchased from a dealer in Erfoud, Morocco in 2006 by Stephan Ralew (Weisberg et al., 2008).

NWA 3163 is a fresh stone that is almost completely coated by a thin, translucent, pale greenish fusion crust (Fig. 1) (Irving et al., 2006). Clasts are visible through the fusion crust. The interior is fresh and pale grey. It is cross-cut by multiple shock veins. Some post-shock

Fig. 1. Photograph of NWA 3163 (1634 g). Cube is 1 cm square. Photo by G. Hupé.

fractures are lined with terrestrial calcite coatings (Irving et al., 2006). NWA 4881 is a broken, irregular stone that is partially covered with a translucent, pale greenish fusion crust. It has a pale brown interior composed of fine-grained, recrystallized plagioclase-rich breccia (Connolly et al., 2007). NWA 4483 consists of 12 broken fragments. The rock is pale gray and fine-grained (<50 μm) (Weisberg et al., 2008).

The similarities among the three stones in mineralogy, texture, and bulk composition, as well as the dissimilarity of this meteorite to other lunar meteorites, support the conclusion made in the original description of NWA 4881 by Connolly et al. (2007) that NWA 3163, 4881, and 4483 are paired stones (i.e., they came from the same parent meteorite, which split up on entering Earth's atmosphere and/or when impacting Earth's surface). At 2.4 kg, NWA 3163 et al. is one of the largest lunar meteorites.

3.2. Mineralogy and texture

The matrices of the meteorites are fine-grained (<50 μm) and consist mostly (>70%) of subrounded anorthite grains with lesser amounts of smaller (<10 μm), rounded mafic minerals concentrated along plagioclase grain boundaries (Fig. 2a). Matrix textures range from poikiloblastic to granoblastic (Fig. 2a and b).

In all samples, numerous mineral clasts and several lithic clasts are embedded in the matrix (Fig. 2c). Some clast boundaries have embayed edges, indicating clast–matrix interaction. Mineral and lithic clasts are more fractured than the matrices of the rocks. Mineral clasts are mostly large (<2 mm) plagioclase crystals that have been shocked to maskelynite, with lesser amounts of pyroxene (<300 μm) and olivine (<75 μm) mineral clasts, and minor spinel-group minerals, ilmenite, and troilite. Fe metal is

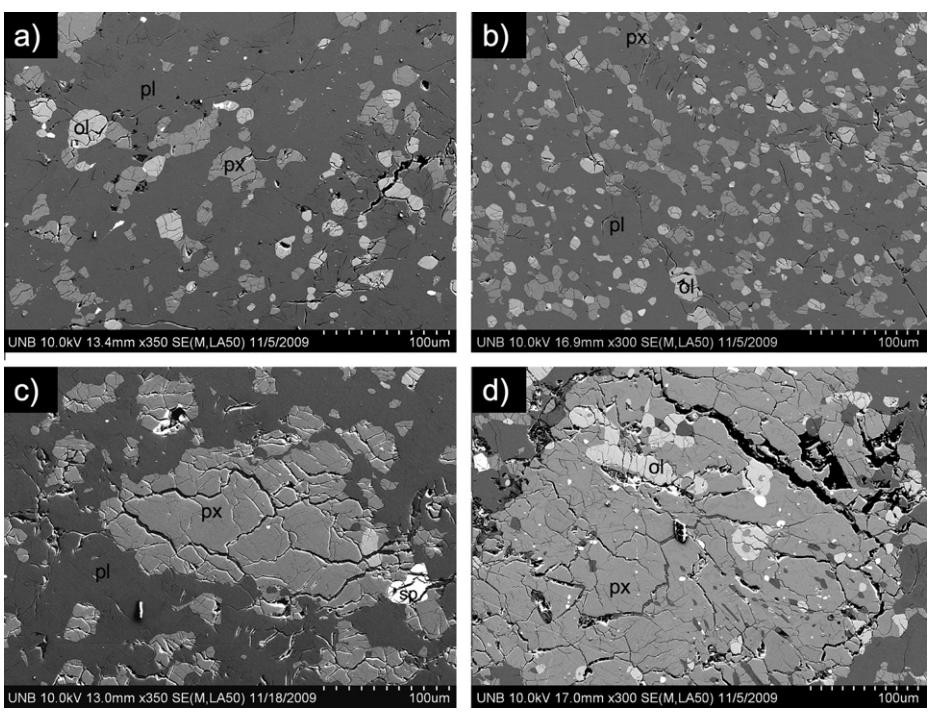

Fig. 2. FE-SEM SE images of textures and minerals observed in samples NWA 3163 et al. (a) The matrix of NWA 3163 ranges from granoblastic to poikiloblastic. A granoblastic portion of the matrix containing mostly plagioclase (pl) with minor olivine (ol) and pyroxene (px) is shown here. (b) A finer-grained portion of the matrix of NWA 4881 containing plagioclase (pl), pyroxene (px), and olivine (ol). Matrix grain size is variable. (c) A large, fractured pyroxene (px) mineral clast in sample NWA 4883. Small spinel (sp) and olivine (lighter gray) grains are enclosed in the larger pyroxene clast. (d) A large, fractured pyroxene (px) lithic clast in NWA 4483. The pyroxene includes rounded olivine (ol), plagioclase (dark gray), and oxides (white).

rare. Metal grains in NWA 3163 et al. are <1 μm, blocky, and are scattered throughout the thin sections. The small size of the metal grains makes them difficult to analyze. A few large (0.5 mm), fractured clasts of olivine are present in NWA 3163 and NWA 4881. Several large (200–300 μm) pyroxene clasts are observed in NWA 3163 and NWA 4881 (Fig. 2d). These clasts are heavily fractured and their edges are embayed. Some pyroxene grains contain round inclusions of plagioclase, olivine, and spinel-group minerals. Several of the large pyroxene clasts contain fine-scale exsolution lamellae, discussed in Section 3.4 (Fig. 3).

Lithic clasts (up to 2 mm^2 in our samples) are distinguished from the matrix based on their larger grain size and their mineralogy (Fig. 4a–d). Many comprise plagioclase (converted to maskelynite by shock) with orthopyroxene, minor olivine, and opaque minerals. The edges of the clasts are round and embayed. The lithic clast population of NWA 3163 includes: (a) two poikiloblastic clasts (1 mm^2) of gabbroic anorthosite, comprising clinopyroxene oikocrysts enclosing rounded plagioclase grains and minor rounded olivine grains, and (b) a cumulate-textured (0.5 mm^2) clast of gabbro. The lithic clast population of NWA 4881 includes: (a) a granoblastic clast of troctolitic anorthosite that is 0.5 mm^2 in size, (b) a 1 mm^2 clast of cumulate-textured gabbro containing large grains of ilmenite, and (c) an ophitic clast of diabase containing clinopyroxene oikocrysts enclosing plagioclase laths and minor blocky spinel-group mineral grains. The lithic population of NWA 4483 includes (a) a granoblastic clast of troctolitic anorthosite that is 0.25 mm^2, and (b) two poikiloblastic clasts (1 and 0.5 mm^2) of gabbroic anorthosite, comprising clinopyroxene oikocrysts enclosing rounded plagioclase grains.

3.3. Shock and weathering effects

The meteorites are heavily shocked and pervasively fractured. Almost all of the plagioclase in the samples has been converted to maskelynite, indicating shock pressures of 28–34 GPa (shock stage S3) (e.g., Hiesinger and Head, 2006, and references therein). Multiple generations of crosscutting fractures are observed in NWA 3163, suggesting that lofting, passage through Earth's atmosphere, and surface impact affected NWA 3163 in different ways. Some fractures are infilled with vesicular melt, which indicates a shock-related injection associated with lunar rather than terrestrial processes (including lofting). Several large melt veins (<100 μm wide) and pockets (<150 μm wide) are observed (Fig. 5a–d). Red staining is present around the edges of NWA 3163, which is probably the product of terrestrial weathering. Irving et al. (2006) observed calcite infilling some veins in NWA 3163. Contamination with Ca-rich material is common in hot-desert meteorites. An unpublished study by A.J.T. Jull reports a cosmogenic ^{14}C age of 12,000 years for NWA 4881, which represents the time that this meteorite spent on Earth.

3.4. Mineral chemistry

Although these meteorites are paired, there are slight geochemical variations among them. This is probably due to lack of statistically adequate sampling, as well as local

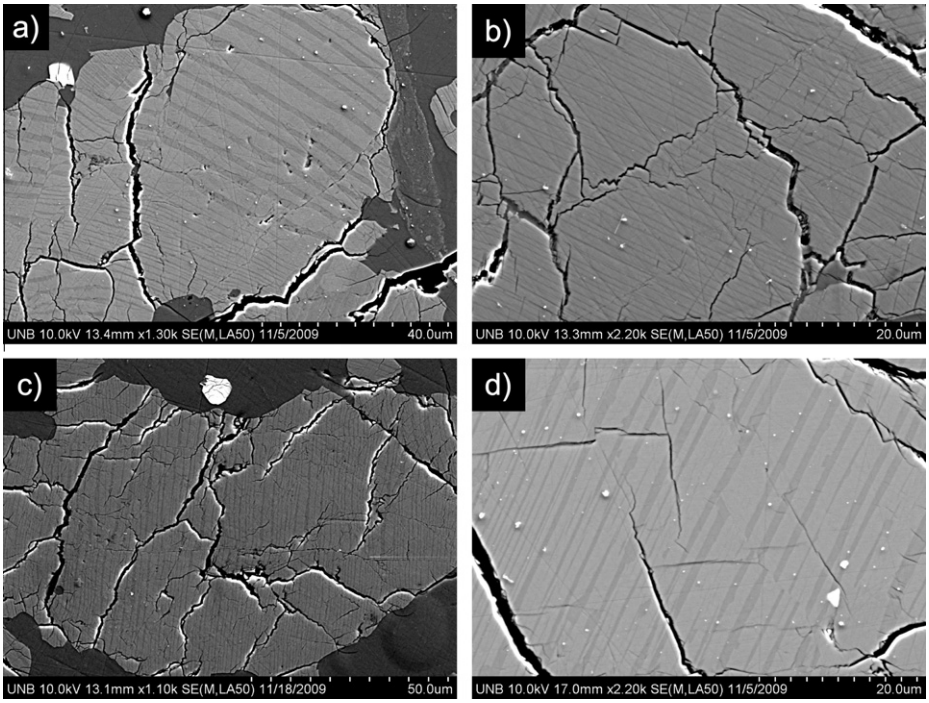

Fig. 3. FE-SEM SE images of pyroxene mineral clasts in (a) NWA 3163, (b) NWA 4881, (c) NWA 4483, and (d) NWA 4881. Exsolution lamellae (subordinate clinopyroxene hosted by orthopyroxene) are apparent in certain larger clasts (as shown here). Some lamellae are curved or offset by microfaults within the mineral grain. Lamellae range up to ~5 μm wide.

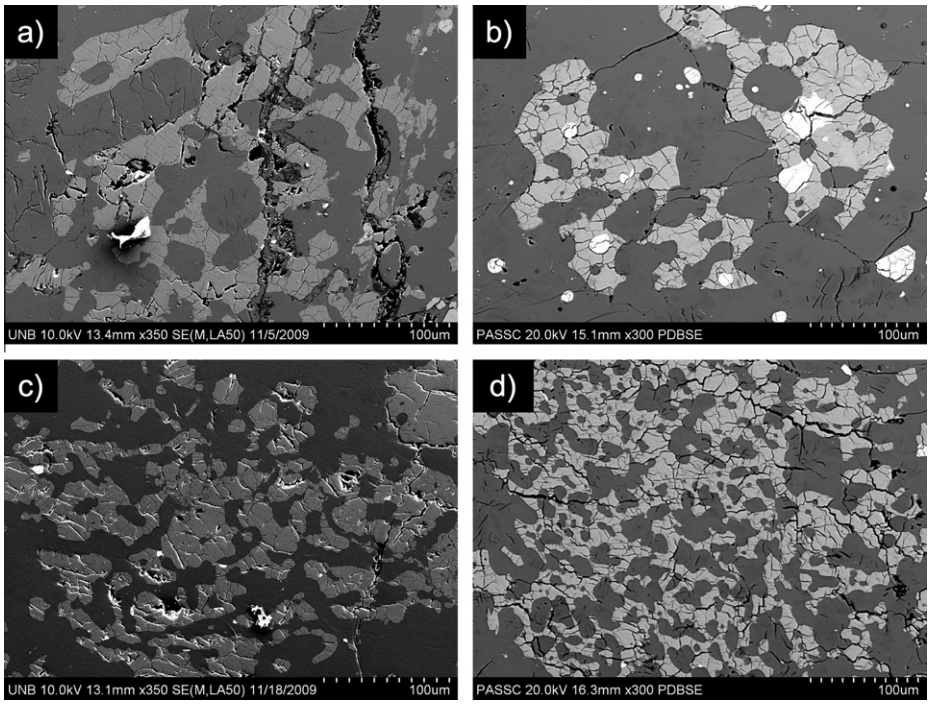

Fig. 4. FE-SEM SE images of poikiloblastic lithic clasts containing pyroxene (light grey) surrounding plagioclase (dark grey) and olivine (white) in (a) NWA 3163, (b) NWA 4881, (c) NWA 4483, and (d) a finer-grained clast in NWA 4881.

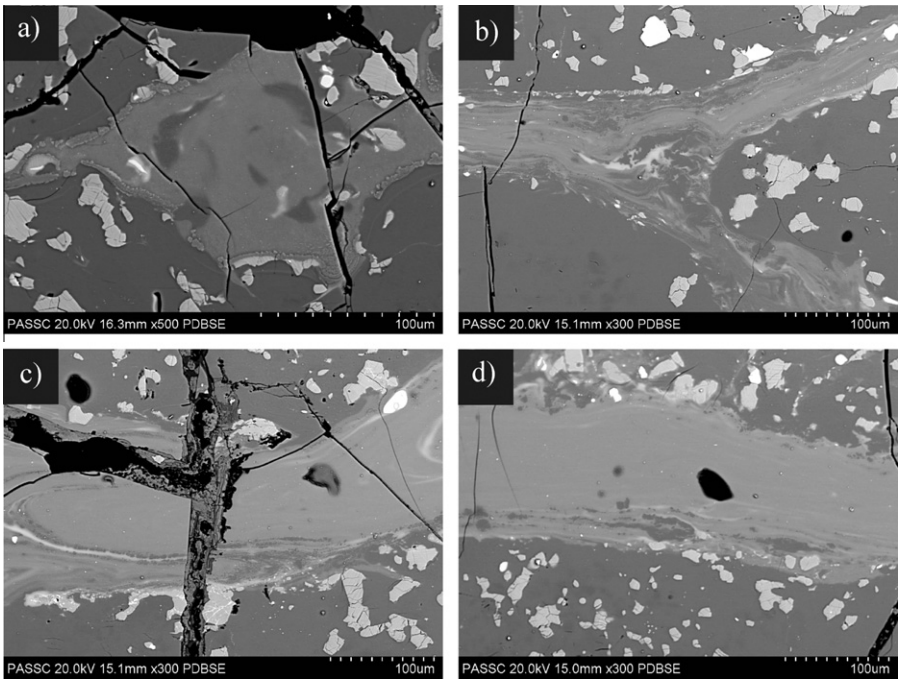

Fig. 5. FE-SEM BSE images of melt veins and pockets in NWA 3163; (a) melt pocket; (b–d) shock veins showing fluidal textures. Note terrestrial phases present in 'vertical' fracture in (c).

compositional variations within the stones. Mineral compositions are ferroan (Mg# 57 for olivine to 67 for orthopyroxene). Representative analyses are presented in Table 1.

Plagioclase from NWA 3163 et al. has largely been converted by shock metamorphism to maskelynite. Plagioclase matrix grains have a compositional range of $An_{95–98}$ with

Table 1
Average mineral compositions for samples NWA 3163 et al.

	A	B	C	D	E	F
SiO_2	44.1	51.8	52.2	52.5	36.2	0.3
TiO_2	b.d.	0.7	0.6	0.5	0.1	52.9
Al_2O_3	35.7	1.6	1.4	1.3	0.1	0.2
Cr_2O_3	b.d.	0.5	0.3	0.2	b.d.	0.4
FeO	0.5	17.3	19.9	21.6	35.1	41.9
MnO	b.d.	0.3	0.4	0.3	0.4	0.3
MgO	0.4	18.6	20.0	21.2	27.1	3.0
CaO	19.5	8.9	5.0	2.2	0.2	0.3
Na_2O	0.4	0.3	0.3	0.3	n.a.	n.a.
K_2O	0.1	0.1	0.1	b.d.	n.a.	n.a.
CoO	n.a.	n.a.	n.a.	n.a.	n.a.	0.1
NiO	b.d.	0.1	0.1	b.d.	0.1	n.a.
Total	100.5	99.9	100.2	100.0	99.4	99.4
Or	0.2					
Ab	3.4					
An	96.4					
Wo		18.5	9.4	4.5		
En		53.5	57.9	60.8		
Fs		28.0	32.7	34.7		
Fo					57.9	
Fa					42.1	
Mg#	–	65.7	63.9	63.6	57.9	11.4
	$n = 32$	$n = 6$	$n = 23$	$n = 2$	$n = 6$	$n = 3$

A, Plagioclase; B, Clinopyroxene; C, Pigeonite; D, Orthopyroxene; E, Olivine; F, Ilmenite.
n.a.: not analyzed; b.d.: below detection limits.

Table 2
Average plagioclase compositions in sample NWA 3163 et al.

	Or	Ab	An	Number
Matrix grains	0.1	3.2	96.7	10
Mineral clasts	0.2	2.8	96.9	4
Inclusions	b.d.	2.8	97.2	2
Lithic clasts	0.3	4.0	95.7	10

an average of An_{97} (Table 2). Mineral clasts range from $An_{96–98}$, with an average of An_{97}. Grains in annealed lithic clasts range from $An_{94–97}$ with an average of An_{96}. Plagioclase is also observed as small (<10 μm), round inclusions in a large (300 μm) orthopyroxene clast (Fig. 2d).

The dominant pyroxene in NWA 3163 et al. is pigeonite (Table 3 and Fig. 6a and b). Orthopyroxene and clinopyroxene are uncommon. Pigeonite matrix grains have compositions of $Wo_{6–15}En_{54–60}Fs_{30–35}$ (average $Wo_8En_{57}Fs_{33}$). Pigeonite mineral fragments exhibit compositions between $Wo_{8–15}En_{53–60}Fs_{32–34}$, with an average composition of $Wo_{10}En_{57}Fs_{33}$. Clinopyroxene mineral clast compositions range between $Wo_{15–29}En_{48–56}Fs_{23–29}$ and average $Wo_{20}En_{53}Fs_{27}$. Two large orthopyroxene grains were analyzed and their compositions range between $Wo_{4–5}En_{60–61}Fs_{34–35}$. Pigeonite is an abundant mineral in lithic clasts with a compositional range of $Wo_{5–13}En_{56–60}Fs_{28–37}$ and an average composition of $Wo_{10}En_{58}Fs_{32}$. Equilibration temperatures for matrix pyroxenes were determined using the Lindsley graphical thermometer (Lindsley, 1983). Temperatures were determined using opx–cpx–pigeonite assemblages for the Lindsley thermometer (Fig. 6a) and using the pigeonite thermometer of Ishii et al. (1976); both of which yield temperatures of 1050 ± 50 °C. The pigeonite thermometer is appropriate for use here because pigeonites are Fe-rich (Fe/(Fe + Mg) = 0.5–0.6) Purity of NWA 3163 et al. pyroxenes exceeds 97 mol% Wo + En + Fs, which renders the need to correcting for the presence of non-quadrilateral components unnecessary (Lindsley, 1983). The effect of these "other" elements is <5 °C (Lindsley, 1983). Temperatures calculated using the pigeonite thermometer of Ishii et al. (1976) gave similar temperatures of ~1090 °C for the pigeonite matrix minerals (Fig. 6c).

Table 3
Average pyroxene compositions for samples NWA 3163 et al.

		Wo	En	Fs	Mg#	Number
Matrix grains	Clinopyroxene	15.1	54.7	30.2	64.4	1
	Pigeonite	8.4	58.4	33.2	63.8	7
Mineral clasts	Clinopyroxene	20.0	52.7	27.3	66.0	4
	Pigeonite	9.6	57.6	32.8	63.7	4
	Orthopyroxene	4.5	60.8	34.7	63.6	2
Lithic clasts	Clinopyroxene	23.8	51.2	25.0	67.4	2
	Pigeonite	9.9	57.7	32.4	64.1	12

Rarely, the larger (typically >100 μm) pyroxene mineral clasts display thin exsolution lamellae of augite (<5 μm) hosted by orthopyroxene (Fig. 3). Intraclast deformation (e.g., Fig. 3a) indicates that they were affected by crushing and shearing prior to peak metamorphism (i.e., they are relict), with both exsolution and microfaulting surviving subsequent heating. Thus, we interpret these particular clasts as representing pre-metamorphic protolith phases that first crystallized as pigeonites, then underwent slow cooling and exsolution. This has implications for the duration of the subsequent "granulite" event in that it was of insufficient duration and temperature to re-homogenize the larger clasts.

Olivine in the matrix exhibits a compositional range between Fo_{56} and Fo_{60} (Table 4). This range is somewhat broader than in other granulitic breccias (Lindstrom and Lindstrom, 1986). Olivine mineral fragments range in composition from Fo_{56} to Fo_{62} and average Fo_{58}. Olivine grains in lithic clasts have an average composition of Fo_{58} and a compositional range between Fo_{57} and Fo_{59}.

Accessory minerals include ilmenite, spinel-group minerals, and troilite. Ilmenite grains exhibit a high MgO content (3 wt%). Spinel-group minerals contain variable amounts of Al_2O_3 (5–15 wt%), TiO_2 (4–21 wt%), Cr_2O_3 (24–44 wt%), and FeO (32–47 wt%) (Fig. 7). The spinel-group minerals are locally intergrown with FeS.

3.5. Bulk chemical composition

Mean compositions of our small bulk samples of NWA 3163, NWA 4483, and NWA 4881 differ somewhat from each other (Tables 5 and 6), but compositions of subsamples of the three stones overlap (Fig. 8). Normatively

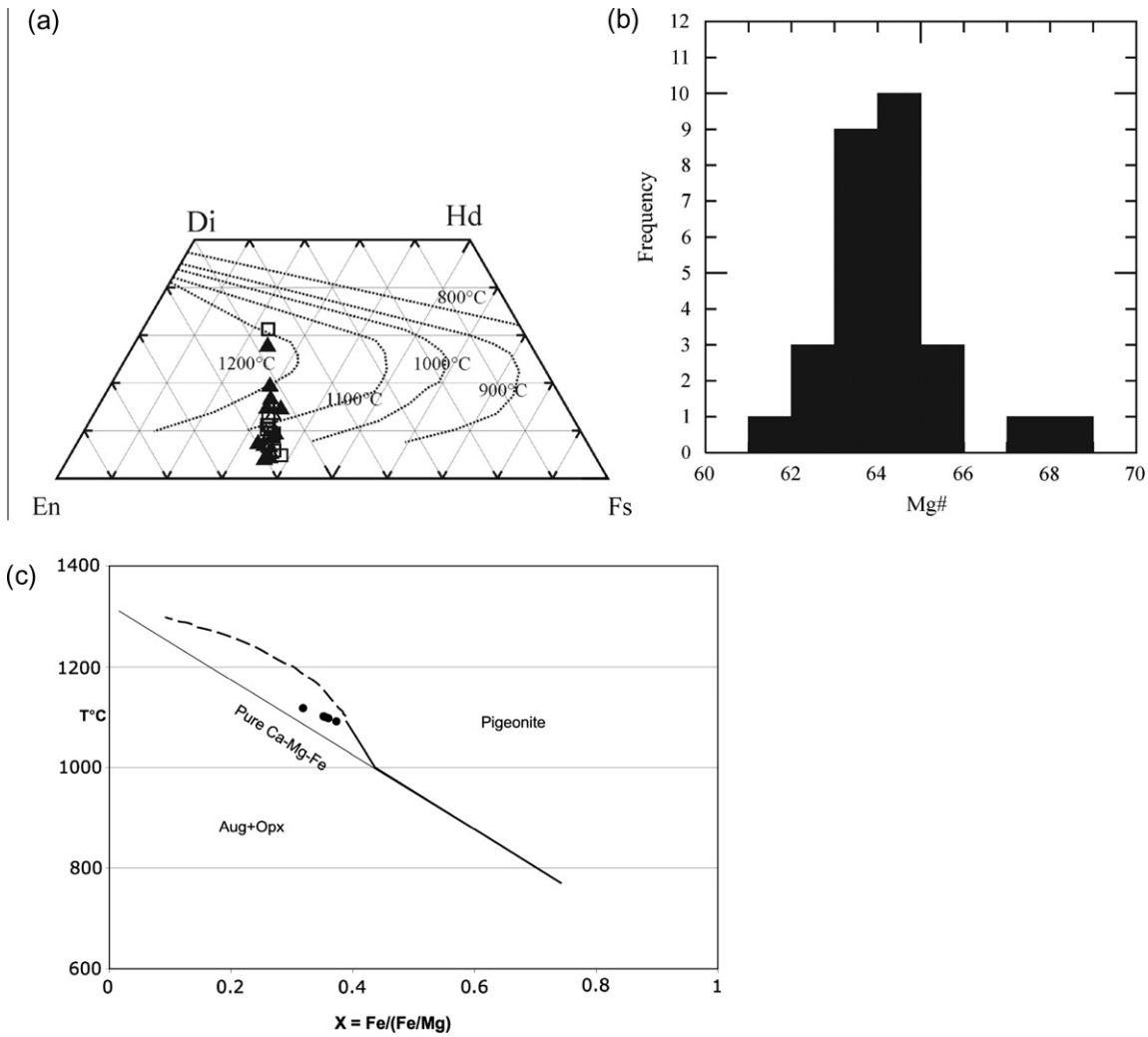

Fig. 6. (a) Pyroxene compositions for NWA 3163 et al. superimposed upon the Lindsley graphical thermometer for P <2 kbar (Lindsley, 1983). Open triangles represent matrix grains, filled triangles represent mineral fragments, and open squares represent grains in lithic clasts. (b) A histogram of Mg' in pyroxene. Mg' falls between 63 and 64. $N = 28$, mean = 64.3, standard deviation = 1.2. (c) Pigeonite thermometer plotting X_{Fe} versus temperature (after Lindsley (1983)). Data (black circles) were calculated using the pigeonite thermometer of Ishii et al. (1976). This diagram gives an approximate minimum crystallization temperature for NWA 3163 et al. The data fall between the pure pigeonite (Pure Ca–Mg–Fe) line and the bold curve, which represents pigeonite co-existing with augite and orthopyroxenes.

Table 4
Average olivine compositions for samples NWA 3163 et al.

	Fo	Fa	Number
Matrix grains	58.2	41.8	7
Mineral clasts	57.8	42.2	16
Inclusions	61.2	38.8	1
Lithic clasts	58.1	41.9	7

(75 wt% plagioclase, or about 79 vol%), the meteorite is a noritic anorthosite (Stöffler et al., 1980). As with other lunar meteorites from northwestern Africa (Korotev et al., 2003, 2009), there is little evidence for contamination with terrestrial Sr (as is common in the Dhofar lunar meteorites); however, our samples of the three stones are significantly contaminated to varying degrees with Ba. NWA 3163 is the least contaminated and NWA 4881 the most contami-

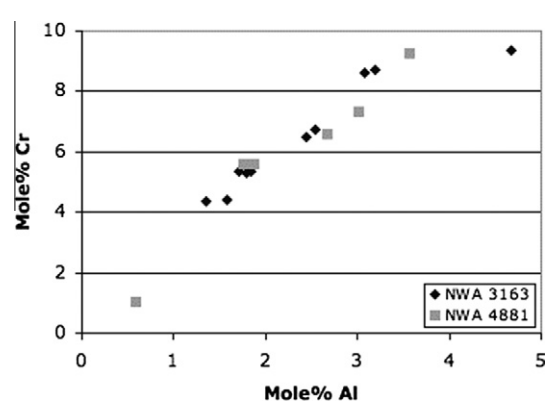

Fig. 7. Spinel-group mineral compositions for samples NWA 3163 and NWA 4881. Compositions represent a continuum between Cr–ulvöspinel and Ti–Al chromite.

Table 5
Average bulk compositions of the five studied granulitic breccia samples taken from the literature and compared to the composition of the feldspathic upper crust and Apollo 17 KREEP.

	60035	77017,2	78115,2	79215,24	NWA 3163 et al.	Feldspathic upper crust[a]	72275,91 A17K
SiO_2	46.49	44.09	45.57	44.8	45.50	44.90	48.00
TiO_2	0.20	0.41	0.27	0.30	0.21	0.22	1.40
Al_2O_3	26.00	26.59	25.94	25.80	25.80	28.50	13.50
Cr_2O_3	0.11	0.13	0.14	0.07	0.19	0.09	0.46
FeO	4.00	6.19	5.82	4.96	6.00	4.00	15.00
MnO	0.05	0.08	0.10	0.06	0.10	0.06	0.16
MgO	8.40	6.06	6.33	8.51	5.86	5.30	10.00
CaO	14.30	15.43	15.18	15.60	15.90	16.40	10.50
Na_2O	0.38	0.30	0.33	0.61	0.28	0.34	0.29
K_2O	0.07	0.06	0.08	0.11	0.03	0.03	0.25
	Ma and Schmitt (1982)	LSPET (1973)	LSPET (1973)	Laul and Schmitt (1973)	Fernandes et al. (2009)	Jolliff et al. (2006)	Papike et al. (1998) and references therein

A17K: Apollo 17 KREEP, typical sample.
[a] Feldspathic upper crust is an estimate of the composition of the upper few kilometers of the crust.

Table 6
Mass-weighted mean results of INAA.

	Unit	Apollo		Dhofar	Dhofar	NWA					
		15418	67215	026	733	3163	4483	4881	mean	±1	±2
Na_2O	%	0.298	0.312	0.325	0.702	0.288	0.292	0.283	0.288	0.003	0.004
CaO	%	16.8	16.8	16.7	15.1	15.8	16.2	15.9	15.9	0.2	0.2
Sc	ppm	7.5	11.4	7.73	3.89	12.6	11.2	14.6	12.8	0.1	1.0
Cr	ppm	537	669	717	359	1025	889	1327	1080	11	133
FeO	%	4.83	5.55	4.35	3.27	5.84	5.01	6.00	5.61	0.06	0.37
Co	ppm	5.31	10.16	16.5	9.88	13.15	12.55	14.54	13.41	0.13	0.6
Ni	ppm	17	29	193	35	38	54	57	50	13	7
Sr	ppm	152	145	238	413	137	143	138	139	11	3
Zr	ppm	<50	<50	32	10	16	13	15	15	23	4
Ba	ppm	14	13	74	89	17	40	86	48	4	19
La	ppm	0.792	0.776	2.58	1.577	0.791	0.921	0.914	0.876	0.015	0.05
Ce	ppm	1.96	1.91	6.65	3.66	2.17	2.48	2.47	2.38	0.13	0.10
Nd	ppm	<5	<5	4.1	2.3	1.6	1.6	0.9	1.3	1.5	0.3
Sm	ppm	0.398	0.482	1.20	0.580	0.489	0.526	0.531	0.516	0.005	0.015
Eu	ppm	0.789	0.736	0.755	1.63	0.658	0.682	0.638	0.660	0.011	0.015
Tb	ppm	0.091	0.122	0.254	0.109	0.123	0.129	0.126	0.126	0.008	0.004
Yb	ppm	0.401	0.545	0.938	0.360	0.548	0.570	0.587	0.569	0.013	0.022
Lu	ppm	0.058	0.080	0.133	0.050	0.081	0.084	0.086	0.084	0.002	0.003
Hf	ppm	0.23	0.29	0.80	0.34	0.33	0.34	0.33	0.34	0.02	0.02
Ta	ppm	0.021	0.034	0.092	0.059	0.043	0.045	0.029	0.039	0.016	0.005
Ir	ppb	<2	<2	7.2	1.3	1.8	1.5	2.3	1.9	0.7	0.7
Au	ppb	<4	<4	9.4	5.0	0.2	1.5	0.4	0.7	0.9	0.4
Th	ppm	0.051	0.067	0.42	0.104	0.099	0.118	0.107	0.108	0.013	0.008
U	ppm	<0.1	<0.1	0.14	0.14	0.04	0.03	0.06	0.04	0.06	0.012
Mass	mg	422	414	326	32	304	314	311	929		
N		4	4	9	2	10	10	9	29		

Each concentration value is the mass-weighted mean of data for *N* subsamples. "Dhofar 026" represents stones Dho 026 (176 mg), Dho 458 (113 mg), and Dho 461 (38 mg). "FeO" is total iron as FeO. The "±1" column contains the estimated analytical uncertainties (1 standard deviation) for the analysis of a single NWA-3163-suite subsample; relative uncertainties for the other are similar. The "±2" column contains the 95% confidence limits ($N = 29$) on the NWA-3163-suite mean data.

nated (e.g., compare NWA 3163 et al. to the Apollo samples in Table 5). The Ba contamination is likely associated with terrestrial calcite infilling the shock veins in the meteorites.

Our results for Dhofar 026 et al. (Table 6) are very similar to those of Warren et al. (2005) (Table 7). Dhofar 733 is distinct and unusual in having the composition of a troctolitic anorthosite (84% normative plagioclase, 12% olivine, and 3% pyroxene), but having concentrations of plagiophile elements (Na, Sr, and Eu) that are about twice the amount typically observed in comparably feldspathic lunar rocks (Korotev et al., 2009). Additionally, the normative albite

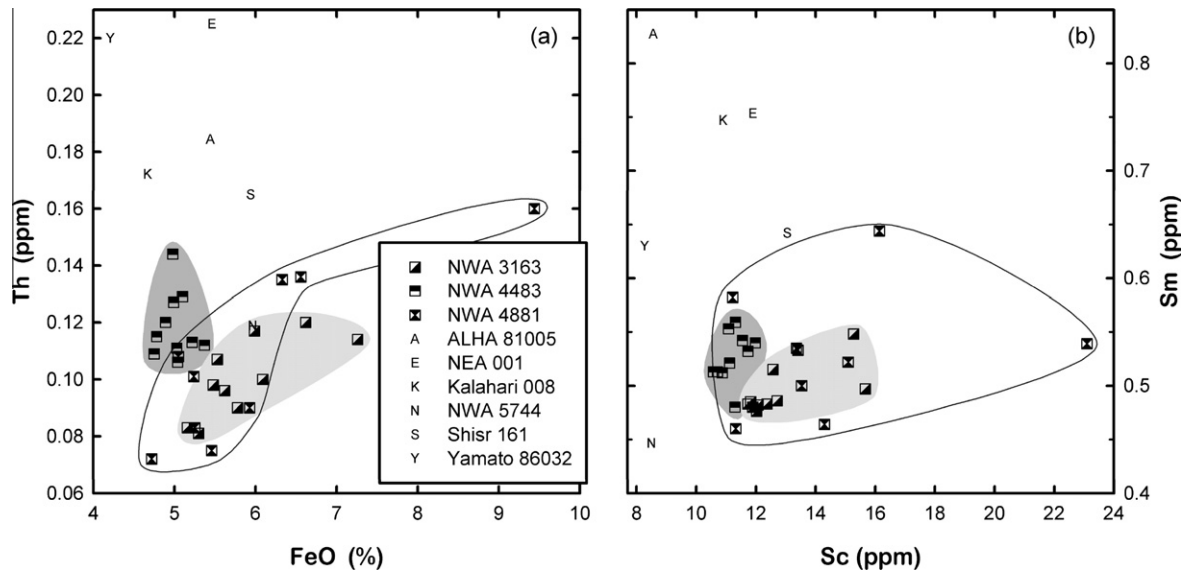

Fig. 8. Comparison of compositions of subsamples of NWA 3163, 4483, and 4881 (squares) to mean composition of other lunar meteorites of similar composition. Subsamples of NWA 4483 are similar to each other in composition whereas those of NWA 4881 are more scattered. There are 19 lunar meteorites with 8–16 ppm Sc (Korotev et al., 2009). Only data for the seven meteorites at the low-Sm end of the range (0.45–6.2 ppm) are plotted here. Data for other meteorites are from Foreman et al. (2009), Koeberl et al. (1989), Korotev and Irving (2005), Korotev et al. (1983, 2009), and Kuehner et al. (2010).

Table 7
Major element data for some granulitic breccias.

	15418	67215	NWA 3163	NWA 4881	Dho 026	Dho 026	Dho 733
SiO_2	44.9	43.9	45.1	45.5	44.2	44.9	44.3
TiO_2	0.27	0.34	0.19	0.21	0.18	0.20	0.27
Al_2O_3	27.3	28.0	27.2	25.8	29.8	29.1	29.8
Cr_2O_3	0.11	0.11	0.150	0.194	0.105	0.083	0.052
FeO	5.95	6.10	5.84	6.00	4.35	4.05	3.31
MnO	0.08	0.09	0.091	0.103	0.061	0.063	0.052
MgO	5.03	5.14	5.01	5.86	4.24	4.06	5.40
CaO	16.1	16.0	16.1	15.9	17.1	16.9	16.2
Na_2O	0.29	0.30	0.288	0.283	0.325	0.302	0.702
K_2O	0.02	0.02	0.023	0.031	0.025	0.036	0.040
P_2O_5	0.03	n.a.	0.022	0.048	0.023	n.a.	0.023
Total	100.0	100.0	100.0	100.0	100.5	99.8	99.3
Mg'	60.1	60.0	60.5	63.5	63.4	64.1	74.4
source	1,3	2,3	3	3	3	4	3

Concentration values in mass%, Mg' in mol%. Sources: (1) Ryder (1985) and Lindstrom and Lindstrom (1986). (2) Lindstrom and Salpas (1981, 1983) and Warren et al. (1990); SiO_2 by difference. (3) This work. "Dho 026" data based on paired stones Dhofar 026, 458, and 461 (mass-weighted mean of analyzed samples); R.A. Zeigler analyst. (4) Warren et al. (2005), based on paired stones Dhofar 026, 457, 458, 459, 461, 462, 463, 464, 465, 466, 467, and 468 (mass-weighted mean of analyzed samples).

content of the plagioclase is Ab_7, compared to the Ab_{3-4} that is characteristic of rocks from the feldspathic highlands.

3.6. ^{40}Ar–^{39}Ar geochronology

The release spectrum of NWA 3163 falls just short of the criteria required for a plateau, but is reproducible (Fig. 9a). The first 10% of the spectrum yields anomalously high (>4.5 Ga) ages caused by contamination by atmospheric (terrestrial) ^{40}Ar, probably associated with degassing of phases altered by exposure on Earth. The analytical errors on individual ages in this low temperature release are large because there is little ^{39}Ar. Ca/K values derived from the low temperature release vary from 39 to 1146, indicative of relatively low Ca phases compared to the rest of the rock (Fig. 9b, Appendix A1). In addition, an isochron plot (Fig. 9c) illustrates the variation from high temperature data points, which form an array yielding an age of 3530 ± 580 Ma, a $^{40}Ar/^{36}Ar$ intercept within errors of 0, and an array of low temperature data points that lie on a mixing trend between that line and a line with similar slope

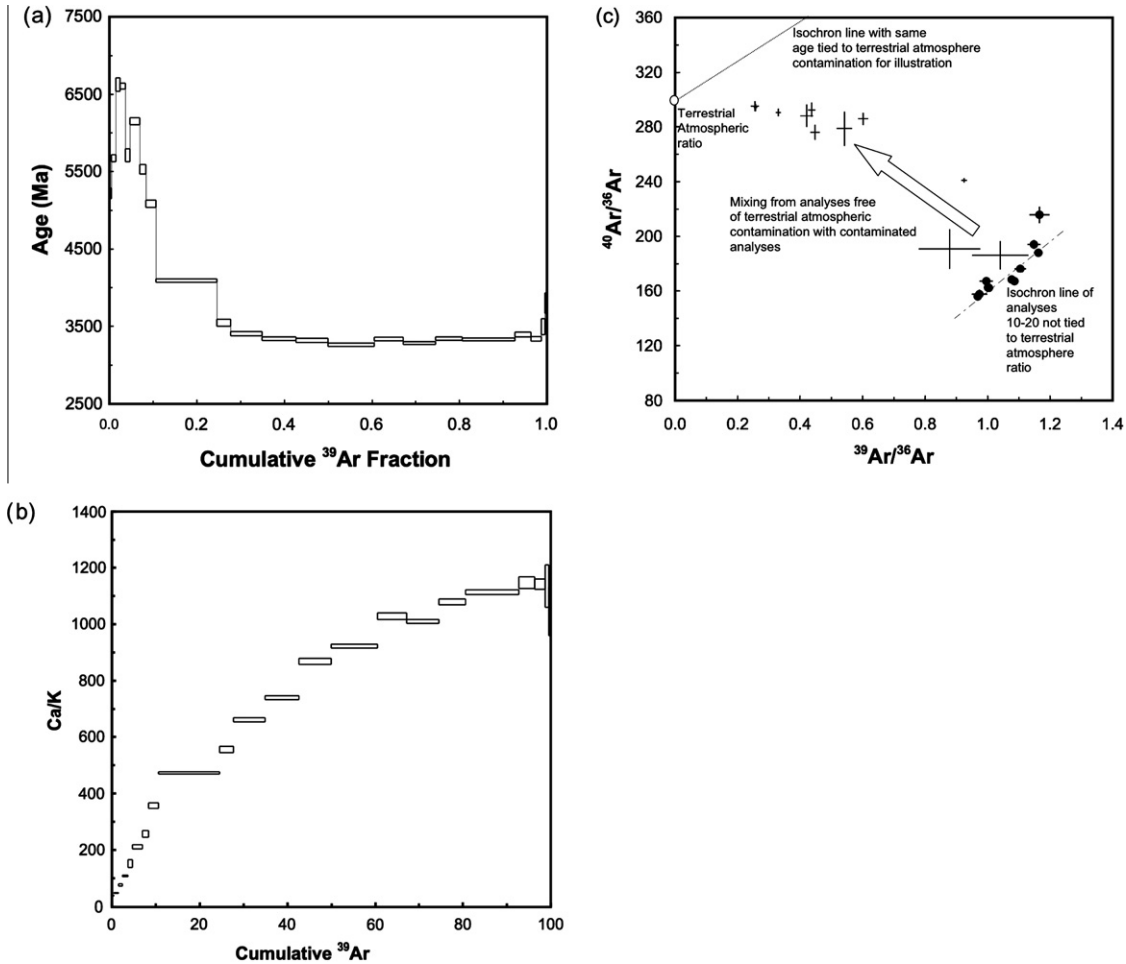

Fig. 9. (a) Step-heating release spectra for meteorite sample NWA 3163 (b) a plot of cumulative ^{39}Ar released versus Ca/K. Box heights are 2σ for both plots. (c) An isochron plot (^{40}Ar/^{36}Ar vs ^{39}Ar/^{36}Ar) illustrating the high temperature points (shown with closed circles) forming an array (but with poor fit and thus high MSWD = 16) and an age of 3530 ± 580 Ma, low temperature data points (shown with no data point marker) on a mixing trend toward the terrestrial atmospheric ^{40}Ar/^{36}Ar ratio of 295.5.

passing through the terrestrial atmospheric ^{40}Ar/^{36}Ar ratio of 295.5. Ignoring the first 10% of the data points that lie in the low temperature array in Fig. 9c, individual release steps for NWA 3163 range in age from 3263 ± 11 Ma to 4087 ± 11 Ma (Fig. 9a). A weighted mean of 11 release steps (steps 11–21 inclusive), between 22% and 98% of the cumulative ^{39}Ar release, yield an age of 3327 ± 29 Ma, which is more precise than the isochron age because it assumes no significant contamination by modern atmospheric argon. This age is reported with 95% confidence.

As with NWA 3163, the first 10% of the release spectrum for NWA 4881 yields very old ages, with some apparent ages being impossible (>4.5 Ga). The high temperature data points of NWA 4881 form an array with an age similar to the step ages although the scatter of the points and lack of a defined intercept means it yields a poorly defined age of 2500 ± 1300 Ma and an intercept within errors of 0. The low temperature data points lie on a mixing trend towards the terrestrial atmospheric ^{40}Ar/^{36}Ar ratio of 295.5, like the previous sample, implying contamination of the low temperature data by modern atmospheric argon. NWA 4881 contains less ^{39}Ar and is more weathered than NWA 3163. Consequently, the data are lower resolution (i.e., there are fewer steps). Its concave age pattern is scattered, but is more similar to that of NWA 3163 than it is to the Apollo granulitic breccia samples (e.g., Hudgins et al., 2008). Ignoring the first 10% of the spectrum, individual release steps for NWA 4881 range from 2562 ± 10 to 3361 ± 14 Ma (Fig. 10a). From 10% to 40%, there is an overall decline in apparent ages to 2562 ± 10 Ma. After 40%, there is a gradual increase in apparent ages until the last step at 3193 ± 24 Ma. ^{37}Ar/^{39}Ar varies from 15–558 and Ca/K content varies from 40 to 1139 (Fig. 10b, Appendix A1).

CRE ages for both samples as determined in this work are within error of each other (Appendix A2). NWA 3163 has a CRE age of 14.5 ± 1.2 Ma and NWA 4881 has a CRE age of 16.0 ± 1.3 Ma. The differences can be attributed to local chemical variations between the analyzed chips, given that the CRE age is determined on the assumption of identical compositions.

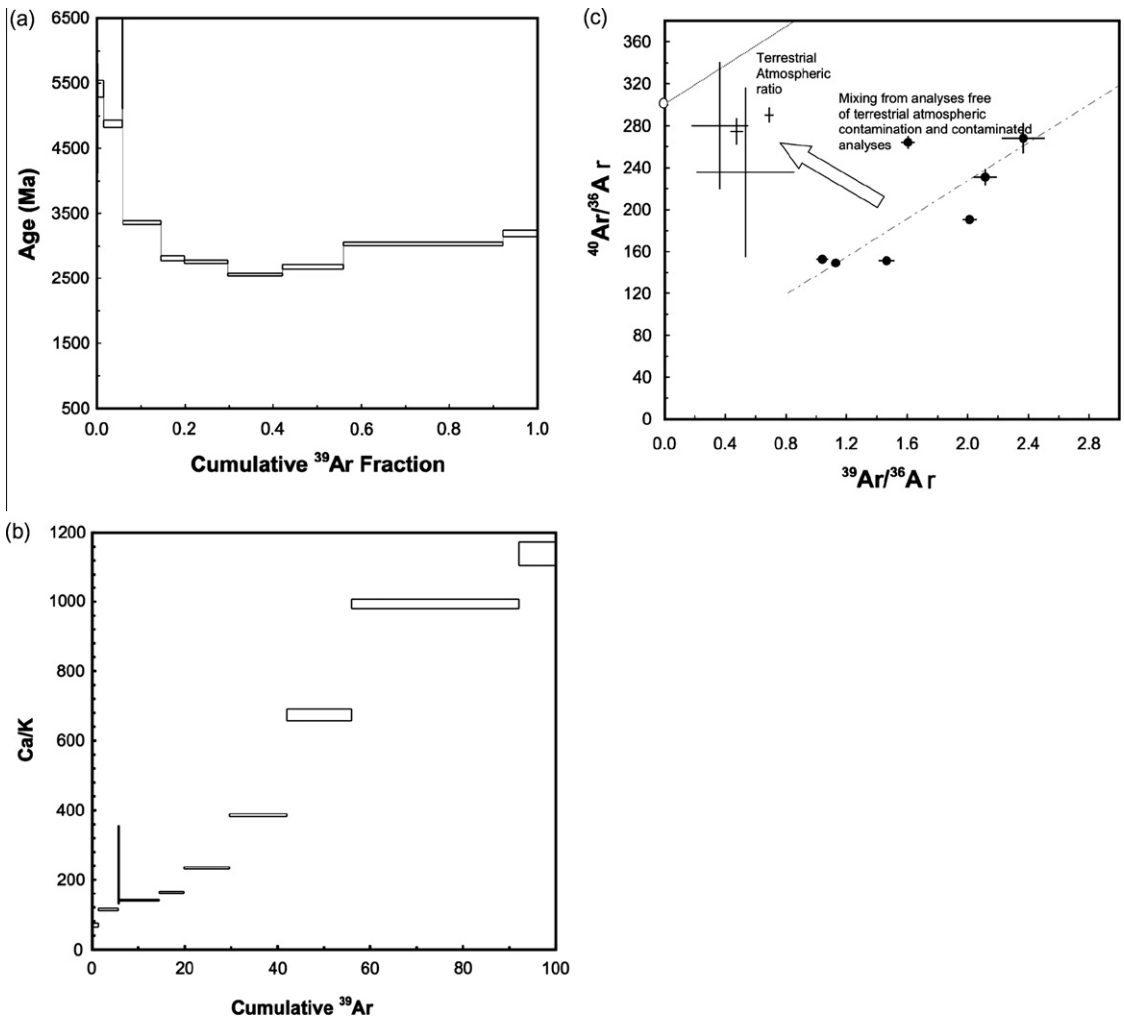

Fig. 10. (a) Step-heating release spectra for meteorite sample NWA 4881, (b) a plot of cumulative ^{39}Ar released versus Ca/K. Box heights are 2σ for both plots. (c) An isochron plot (^{40}Ar/^{36}Ar vs. ^{39}Ar/^{36}Ar) illustrating the high temperature points (shown with closed circles) forming an array (but with poor fit and thus high MSWD = 150) and an age of 2500 ± 1300 Ma, low temperature data points (shown with no data point marker) on a mixing trend toward the terrestrial atmospheric ^{40}Ar/^{36}Ar ratio of 295.5.

4. COMPARISONS TO OTHER GRANULITIC BRECCIAS

4.1. Petrography and petrology

Like the four Apollo granulitic breccias of our previous study, Apollo 16 sample 60035 and Apollo 17 samples 77017, 78155, and 79215 (Hudgins et al., 2008), the meteorites have metamorphic-textured matrices that are either granoblastic, poikiloblastic, or intermediate between the two. All have similar mineralogy: 70–80% high-Ca plagioclase, with lesser amounts of olivine and pyroxene, and minor amounts of oxides and other accessory minerals. All were last equilibrated at 1050 ± 50 °C, according to two-pyroxene thermometry, a range we interpret to be the minimum temperature of the peak thermal metamorphism that was responsible for annealing and recrystallizing the precursor rocks (i.e., the "granulite" event).

Mineralogical differences include (1) the absence of large Fe–Ni metal grains in the studied meteorites, and (2) the widespread presence of maskelynite in the meteorites, which is uncommon in the Apollo granulitic breccias. The presence of maskelynite in the meteorites indicates that they were exposed to higher shock pressures (>28 GPa) than the Apollo samples. Shock effects in the Apollo granulitic breccias suggest pressures of 5–22 GPa (Hudgins et al., 2008). Plagioclase in other granulitic breccia meteorites (e.g., Dho 026 (James et al., 2003), Dho 733 (Foreman et al., 2008), and NWA 5744 (Kuehner et al., 2010)) was also partially or completely converted to maskelynite. NWA 3163 et al. contain melt pockets and shock veins, which are rare to absent in the Apollo samples, but have been noted in Dho 026, another granulitic breccia meteorite (James et al., 2003). The development of higher shock pressure conditions within the lunar meteorites, but not the directly sampled Apollo and Luna samples, suggests that impact

conditions specifically associated with lofting are responsible for the enhanced shock effects.

4.2. Chemical composition

Granulitic breccias range in composition from anorthosite (sample 674883 of Stöffler et al., 1985, with 94% normative plagioclase) to anorthositic troctolite (clast D2 from Dhofar 309 of Treiman et al., 2010, with 59% normative plagioclase; Fig. 11). Mg' (whole-rock mol% MgO/[MgO + FeO]) covers a wide range, from 55 to 88. On the basis of the Apollo samples, Lindstrom and Lindstrom (1986) advocated that granulitic breccias were dichotomous, with ferroan (Mg' <65) and magnesian (Mg' >72) groups. The dichotomy is not evident in Fig. 11, where the data appear to be consistent with a continuum. NWA 3163 et al. and Dhofar 026 are ferroan, nonetheless, and Dhofar 733 and NWA 5744 are magnesian.

For incompatible elements, the four granulitic breccia meteorites are at the low end of the concentration range observed among the Apollo granulites (Fig. 12a). Given that, on statistical grounds, most of the lunar meteorites must originate from points distant from the Procellarum KREEP Terrane (Korotev et al., 2009), this observation implies that most Apollo granulitic breccias, and perhaps Dhofar 026, are slightly contaminated by KREEP, whereas most of the granulitic-breccia meteorites are not (Fig. 12a). Korotev et al. (2003) noted that Apollo magnesian granulitic breccias have Th/Sm ratios distinctly greater than chondritic. This characteristic is lacking in the meteorites, which tend to have chondritic Th/Sm (Fig. 12b). These differences may reflect lateral variation in the crust, possibly related to proximity of Apollo 16 and 17 to the Procellarum KREEP Terrane.

As noted by Haskin et al. (1998), granulitic breccias from Apollo 17 are rich in siderophile elements. These elements are carried by Fe–Ni metal grains, such as those we reported in Hudgins et al. (2008) for samples 77017, 78155, and 79215. Metal grains in NWA 3163 et al. are rare and bulk rock concentrations of Ni, Ir, and Au are consequently much lower than in the Apollo 17 samples (Table 5 and Fig. 12c). Low to moderately low concentrations of siderophile elements (e.g., <150 ppm Ni) are typical of granulitic breccias, with only those from Apollo 17 and

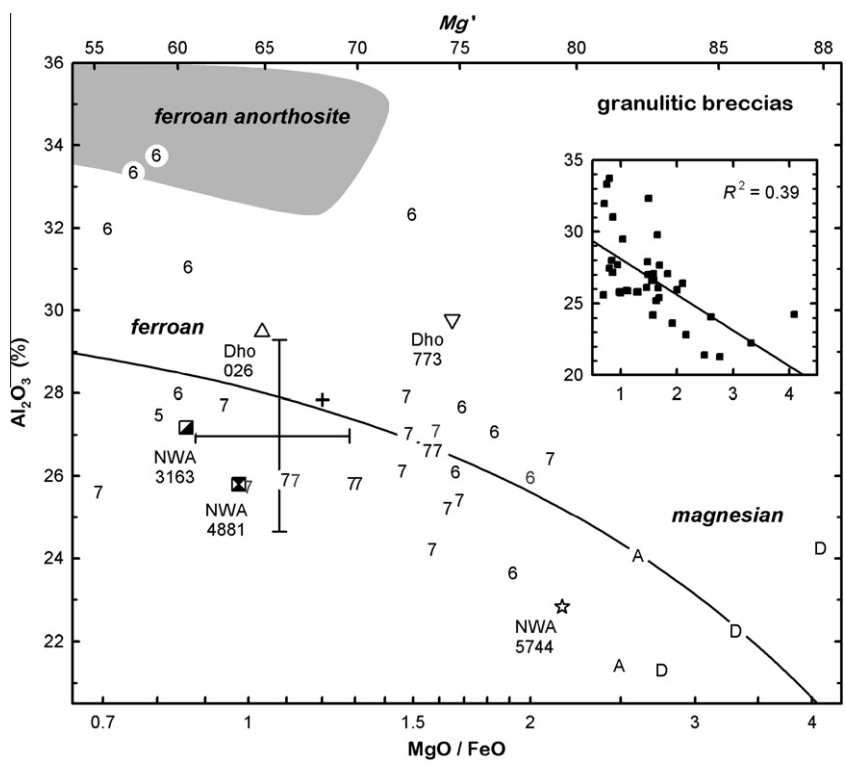

Fig. 11. Bulk compositions of granulitic breccias and comparison of granulitic breccias among the lunar meteorites (geometric symbols) to those from Apollo 15 (5), 16 (6), and 17 (7); see Fig. 12 for sources of data. Each point represents a different sample, except for A and D, which represent clasts in lunar meteorites ALHA 81005 and Dhofar 309, respectively (Treiman et al., 2010). Apollo pristine ferroan anorthosites plot in the gray field, which extends off scale to $Mg' = 44$ (data from Warren, 1993; pristinity index >6). The large crossed error bars represent the mean and standard deviation of lunar meteorites ($N = 19$) plotting in the range of this figure that are regolith breccias and fragmental breccias (i.e., those meteorites representing material from the surface of the feldspathic highlands) (data of Foreman et al., 2009; Hidaka et al., 2009; and Korotev et al., 2003, 2006, 2009). If that material contains as much as 5% mare basalt, on average (almost certainly an upper limit), then the nonmare component would plot at the small plus (+) symbol. See Fig. 12 for sources of data. The inset shows the data on a linear scale; the line represents a simple least-squares fit to the data.

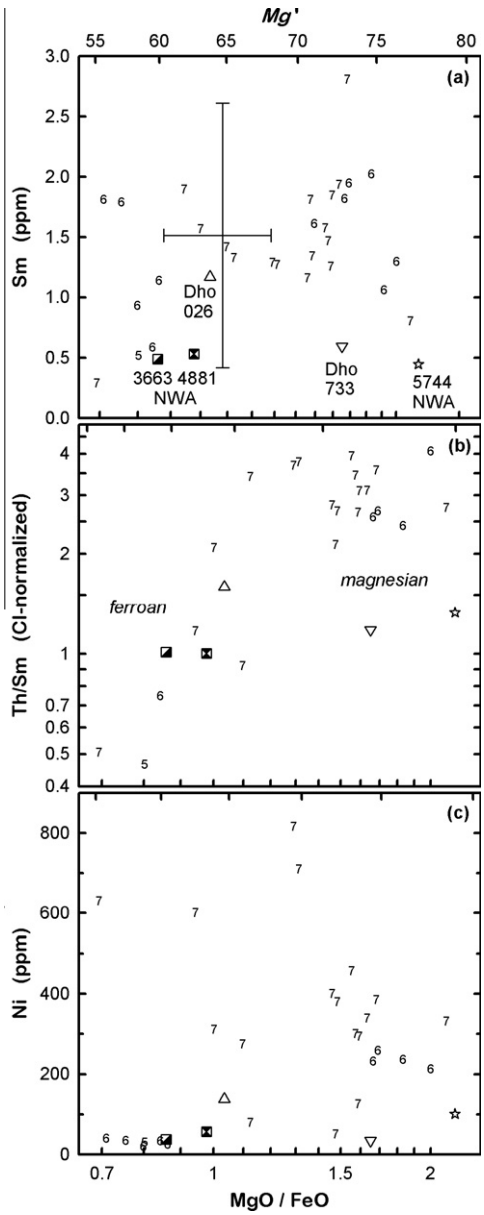

Fig. 12. Comparison of the lunar meteorite granulitic breccias (geometric symbols) with those from Apollo 15 (5), 16 (6), and 17 (7). (a) The three Apollo samples plotting closest to NWA 3663 and NWA 4881 are 15418, 67215, and 76503, 7084 (Jolliff et al., 1996). Most Apollo granulitic breccias are richer in REE than the meteorites. The large crossed error bars are the same as those of Fig. 11. In order to raise Sm from the 0.5 ppm of NWA 3663 and NWA 4881 to the 1.15 ppm of Dhofar 026 or 2.0 ppm of the typically highest Apollo 16 and 17 samples would require 1.4–3.2% KREEP with 48 ppm Sm (Warren, 1989). (b) Magnesian granulitic breccias from Apollos 16 and 17 have high Th/Sm (Korotev et al., 2003), but this tendency is not observed among the meteorites. (c) Apollo granulitic breccias, particularly those from Apollo 17, tend to be rich in siderophile elements. Data from Bansal et al. (1972), Laul et al. (1972, 1974), Laul and Schmitt (1973a,b), Hubbard et al. (1974), Boynton et al. (1976), Wänke et al. (1976), Blanchard et al. (1977), Lindstrom et al. (1977), Wasson et al. (1977), Palme et al. (1978), Ma and Schmitt (1982), Lindstrom and Salpas (1981, 1983), Stöffler et al. (1985), Lindstrom and Lindstrom (1986), Warren et al. (1990, 2005), Foreman et al. (2008), Kuehner et al. (2010), and this work.

some from Apollo 16 having higher concentrations (Fig. 12c).

The only systematic feature found among the Apollo and meteoritic granulitic breccias is the tendency for granulites at the mafic (low Al_2O_3) end of the range to be more magnesian (greater MgO/FeO) than those at the anorthositic (high Al_2O_3) end of the range (Fig. 11). Lunar meteorites that are regolith and fragmental breccias (Fig. 11) have been used to estimate the composition of the feldspathic upper crust of the Moon because they consist of well-mixed surface material from randomly distributed locations in the feldspathic highlands (Palme et al., 1991; Korotev et al., 2003). Several ferroan granulitic breccias, including NWA 3163 et al. and Dhofar 026, have compositions in the range of such estimates (Figs. 11 and 12a). Thus, the compositions of NWA 3163 et al., and some other ferroan granulitic breccias, are consistent with derivation from typical material of the upper crust of the feldspathic highlands, perhaps regolith or megaregolith. Most magnesian granulitic breccias are not consistent with this scenario, however, because they are more mafic and more magnesian. The most magnesian feldspathic regolith samples known are Apollo 16 sample 67960 (Korotev, 1996) and meteorite ALHA 81005 (Korotev et al., 2006), both with $Mg' = 73$, which is at the low end of the range of magnesian granulitic breccias. ALHA 81005 is an impact-generated mixture containing both highly ferroan and highly magnesian lithologies (Korotev et al., 1983; Simon et al., 1983; Treiman and Drake, 1983; Goodrich et al., 1984; Treiman et al., 2010). At Apollo 16, the ferroan regolith samples were collected within a few hundred meters of magnesian sample 67960 (Korotev, 1996). There are several implications of these observations. It is unlikely that magnesian granulitic breccias ($Mg' > 75$) are metamorphosed regolith because regolith samples are not so magnesian. The protolith of the magnesian granulitic breccias must derive from deeper in the Moon than the regolith. Finally, if most regolith samples are ferroan, then there are at least some places in the feldspathic highlands where magnesian anorthositic troctolite, perhaps as intrusions (Korotev et al., 2003; Treiman et al., 2010), underlie ferroan-anorthositic-suite rocks. However, it is not clear whether ferroan granulitic breccias, such as NWA 3163 et al., actually form from regolith/megaregolith, as allowed by Figs. 11 and 12a, or simply originate from regions of the feldspathic highlands where magnesian material does not occur.

4.3. ^{39}Ar–^{40}Ar ages

The authors have previously published an investigation of four Apollo granulitic breccias: Apollo 16 sample 60035 and Apollo 17 samples 77017, 78155, and 79215 (Hudgins et al., 2008). $^{40}Ar/^{39}Ar$ data reveal that 60035, 77017, and 78155 have peak metamorphic ages of 4.1 Ga, while 79215 has a peak metamorphic age of 3.9 Ga. NWA 3163 et al. are much younger than the Apollo granulitic breccia samples. The results of this study reveal that NWA 3163 et al. underwent heating

at 3300–3500 Ma, with partial resetting at ~2000–2500 Ga or younger.

Fernandes et al. (2009 and associated poster) report a plateau age for NWA 4881 of 3478 ± 41 Ma, which is slightly older than our mean age of 3327 ± 29 Ma for paired stone NWA 3163. However, the shapes of the two spectra for NWA 4881 are very similar, indicating comparable thermal histories. Like our experiment, Fernandes et al.'s NWA 4881 spectrum dips to lower ages (~1950 Ma), then climbs back to ~3400–3500 Ma. Some of the differences between the two results can be attributed to Fernandes et al.'s higher resolution heating schedule. However, both data sets point to a main event at 3300–3500 Ma that completely reset the argon chronometer of NWA 4881. The age of NWA 3163 falls within this range and looks like an unreset version of 4881. We equate this main event with peak metamorphism and complete resetting (i.e., the "granulitic" event). Differences in Ar spectra between NWA 3163 and 4881 can be attributed to minor compositional variations in the analyzed samples, and differences in shock and weathering effects at the micro-scale.

Although the Ar–Ar ages we obtained from the Apollo granulitic breccia (79215 in particular) suite hint at either formation during, or subsequent overprinting from, the late heavy bombardment (LHB) period (~3.8–4.0 Ga), Ar–Ar spectra from NWA 3163 et al. are younger and thus yield no evidence for the Late Heavy Bombardment. A compilation of ages for lunar granulites (Hudgins et al., 2008) shows metamorphic cooling ages for the Apollo samples fall dominantly in the region 3.8–4.1 Ga and thus the samples in the present study (NWA 4881 and NWA 3163) yield the youngest cooling ages for lunar granulites detected thus far, perhaps as a result of sampling a region that is geologically distinct from the Apollo sites.

5. SUMMARY

(1) Geochemical, mineralogical, and textural evidence indicates that the lunar granulitic breccias NWA 3163, 4881, and 4483 are three stones derived from a common parent meteorite.
(2) The Apollo and meteorite granulitic breccias are texturally similar and have comparable bulk compositions and equilibration temperatures (1000–1100 °C). However, the trace and siderophile element contents of the meteorites point to distinct parental lithologies derived from different regions of the Moon (i.e., outside the region that the Apollo missions sampled, so beyond the PKT).
(3) Our results reveal that NWA 3163 et al. underwent heating to 1000–1100 °C (responsible for the main metamorphic "granulitic" recrystallization texture) at 3300–3500 Ma, with partial resetting at ~2560 Ma or younger. Differences in Ar spectra between NWA 3163 and 4881 can be attributed to minor compositional variations in the analyzed chips and to differences in shock and weathering effects at the micro-scale.
(4) The parental rocks of the Apollo and meteorite samples underwent similar high temperature-low pressure metamorphic conditions but in separate areas of the Moon and at different times in lunar history. Coupled with the implied younger ages of NWA 3163 et al., this indicates that lunar granulitic breccias are the products of a common formation process, rather than being derived from a particular region at a particular time in the Moon's evolution.
(5) Shock effects (28–34 GPa) are manifest in the lunar granulitic breccia meteorites, but are limited in most Apollo samples (5–22 GPa). Shock features in the meteorites include the development of maskelynite, shock veins, and melt pockets. Shock is attributed to the lofting event, thus distinguishing the meteorites from unlofted Apollo material.
(6) With 75% normative plagioclase and a Mg' of 62, NWA 3163 et al. derive from ferroan-anorthositic-suite rocks of the feldspathic highlands that are considerably more mafic than ferroan anorthosites of the Apollo collection.
(7) The relative depletion in siderophiles shown by the NWA et al. compared to the Apollo samples favors less interaction with siderophile-bearing impactors. Either the metamorphic event at ~3.4 Ga completely erased evidence of 3.8–4.0 Ga (Late Heavy Bombardment or LHB) ages, or the parental rocks of the meteorites were formed after LHB processing.

ACKNOWLEDGMENTS

This work was supported by a Natural Sciences and Engineering Research Council of Canada (NSERC) CGS D-3 grant and a J.S. Little Travel Fellowship to JAH, NSERC, and Canada Research Chair grants to JGS, and NASA Grant NNX07AI44G to RLK. SPK gratefully acknowledges funding from the Leverhulme Trust (F/002 69/J) and James Schwanethal for help in the analyses. We thank M. Altman, W. Hsu, A.J. Irving, L. Labenne, and S. Ralew for samples of the lunar meteorites, R.A. Zeigler for major-element analysis, and Jisun Park, Jeff Taylor, Nicolle Zellner, and an anonymous reviewer for their constructive comments on an earlier version of the manuscript. PASSC contribution 67.

APPENDIX A

See Appendix Tables A1 and A2.

Appendix Table A1
Infrared stepped-heating ages for NWA 3163 and 4881.

	^{40}Ar	±	^{39}Ar	±	^{38}Ar	±	^{37}Ar	±	^{36}Ar	±	%^{39}Ar	Ca/K	$^{40}Ar^{*}/^{39}Ar$	±	Age	±
NWA 3163	$J = 0.03314$															
Step 1	149.504	2.075	0.291	0.004	0.099	0.019	5.393	0.038	0.536	0.010	0.441	38.588	514.301	10.050	5218.757	34.371
Step 2	468.518	2.240	0.700	0.007	0.342	0.020	16.160	0.038	1.601	0.012	1.504	48.042	669.621	7.801	5671.518	21.884
Step 3	701.060	2.226	0.605	0.015	0.446	0.019	22.247	0.038	2.373	0.012	2.423	76.448	1158.224	28.120	6626.906	43.583
Step 4	918.701	2.031	0.802	0.007	0.639	0.022	41.800	0.038	3.120	0.012	3.642	108.357	1144.972	10.906	6606.675	18.909
Step 5	458.698	4.234	0.670	0.014	0.325	0.012	48.882	1.936	1.592	0.018	4.659	151.731	684.522	15.878	5709.528	41.000
Step 6	1321.697	3.909	1.500	0.018	1.001	0.013	152.088	1.938	4.546	0.018	6.937	210.878	881.059	10.636	6147.812	22.791
Step 7	567.821	3.599	0.921	0.014	0.529	0.013	113.776	1.939	2.057	0.016	8.336	256.974	616.577	10.318	5529.309	30.040
Step 8	719.185	3.678	1.513	0.018	0.969	0.013	259.777	1.940	2.516	0.016	10.634	357.053	475.235	6.029	5084.438	23.132
Step 9	2380.302	3.819	9.134	0.036	6.149	0.024	2075.656	1.941	9.878	0.029	24.505	472.666	260.596	1.109	4087.088	10.615
Step 10	386.779	3.692	2.090	0.020	1.509	0.013	557.912	1.942	1.793	0.018	27.679	555.233	185.058	2.506	3544.399	22.390
Step 11	797.564	3.678	4.717	0.026	3.942	0.016	1497.686	1.944	4.109	0.028	34.842	660.454	169.092	1.220	3405.352	13.438
Step 12	825.137	3.696	5.097	0.023	4.886	0.024	1814.516	1.944	4.386	0.016	42.582	740.501	161.893	1.041	3338.964	12.383
Step 13	769.299	3.670	4.817	0.030	5.090	0.027	2011.920	1.946	4.361	0.023	49.897	868.833	159.719	1.242	3318.433	14.025
Step 14	1071.967	3.678	6.966	0.025	8.163	0.024	3090.086	1.946	6.414	0.023	60.476	922.645	153.880	0.762	3262.086	10.613
Step 15	699.523	0.641	4.334	0.025	5.694	0.021	2143.287	0.332	4.315	0.016	67.057	1028.678	161.413	0.935	3334.448	11.632
Step 16	771.033	0.873	4.936	0.017	6.095	0.024	2396.316	0.332	4.584	0.019	74.553	1009.756	156.200	0.552	3284.687	9.260
Step 17	648.223	0.781	3.996	0.019	5.379	0.024	2072.724	0.332	3.991	0.014	80.622	1078.848	162.211	0.784	3341.948	10.578
Step 18	1282.727	0.912	7.968	0.030	10.856	0.031	4265.114	0.332	8.226	0.028	92.723	1113.339	160.978	0.626	3330.356	9.624
Step 19	398.339	0.382	2.373	0.021	3.279	0.016	1308.517	0.332	2.384	0.014	96.327	1146.901	167.856	1.493	3394.123	15.603
Step 20	258.078	0.370	1.595	0.012	2.113	0.028	875.335	0.332	1.638	0.016	98.749	1141.670	161.828	1.287	3338.355	14.282
Step 21	94.748	0.247	0.529	0.017	0.732	0.013	288.636	0.333	0.509	0.014	99.552	1134.570	179.056	5.932	3493.375	51.723
Step 22	64.074	0.219	0.295	0.012	0.478	0.016	148.274	0.333	0.336	0.013	100.000	1046.096	217.333	8.990	3796.466	66.001
NWA 4881	$J = 0.03311$															
Step 1	0.303	0.134	n.d.	n.d.	n.d.	n.d.	n.d.	n.d.	n.d.	n.d.	n.d.	n.d.	n.d.	n.d.	n.d.	n.d.
Step 2	11.047	0.143	0.025	0.006	0.017	0.007	0.484	0.070	0.047	0.008	0.136	40.233	441.779	110.836	4959.574	423.740
Step 3	96.191	0.161	0.166	0.006	0.070	0.009	5.566	0.070	0.350	0.008	1.402	69.573	578.102	21.790	5417.335	65.189
Step 4	233.702	0.214	0.555	0.009	0.163	0.007	30.501	0.070	0.805	0.010	5.626	114.248	420.852	6.727	4877.755	28.190
Step 5	20.772	0.138	0.027	0.006	0.010	0.007	3.139	0.070	0.074	0.008	5.831	242.719	772.266	179.961	5917.097	404.675
Step 6	186.377	0.203	1.133	0.009	0.274	0.009	76.241	0.070	0.706	0.008	14.452	139.933	164.460	1.299	3361.743	14.246
Step 7	79.996	0.161	0.706	0.009	0.188	0.007	55.135	0.070	0.298	0.008	19.820	162.510	113.359	1.442	2812.381	19.469
Step 8	140.328	0.379	1.284	0.009	0.410	0.009	144.443	0.070	0.607	0.010	29.591	233.941	109.267	0.810	2760.214	12.643
Step 9	155.085	0.175	1.637	0.009	0.879	0.009	303.592	0.070	0.814	0.008	42.041	385.847	94.761	0.527	2562.081	10.233
Step 10	188.379	0.351	1.823	0.022	1.541	0.009	590.690	0.070	1.245	0.016	55.906	674.133	103.360	1.284	2682.143	18.693
Step 11	629.172	0.362	4.761	0.034	5.937	0.012	2274.541	0.070	4.218	0.013	92.127	993.664	132.145	0.940	3034.248	12.772
Step 12	152.242	0.206	1.035	0.015	1.569	0.015	566.962	0.070	0.996	0.010	100.000	1139.460	147.101	2.206	3193.226	23.661

Appendix Table A2
CRE ages for NWA 3163 and 4881.

Sample	J	37 at 1.54	$^{38}Ar/^{37}Ar$	$^{38}Ar/Ca$	CRE age (Ma)	±
NWA 3163	0.03312	650	0.002369	2.75E-07	14.5	1.2
NWA 4881	0.03312	590	0.002610	3.03E-07	16.0	1.3

REFERENCES

Bansal B. M., Church S. E., Gast P. W., Hubbard N. J., Rhodes J. M. and Wiesmann H. (1972) The chemical composition of soil from the Apollo 16 and Luna 20 sites. *Earth Planet. Sci. Lett.* **17**, 29–35.

Blanchard D. P., Jacobs J. W. and Brannon J. C. (1977) Chemistry of ANT-suite and felsite clasts from consortium breccia 73215 and gabbroic anorthosite 79215. *Proc. Lunar Sci. Conf.* **8**, 2507–2524.

Boynton W. V., Chou C.-L., Bild R. W., Baedecker P. A. and Wasson J. T. (1976) Element distribution in size fractions of Apollo-16 soils: evidence for element mobility during regolith processes. *Earth Planet. Sci. Lett.* **29**, 21–33.

Cohen B. A., James O. B., Taylor L. A., Nazarov M. A. and Barsukova L. D. (2004) Lunar highland meteorite Dhofar 026 and Apollo sample 15418: two strongly shocked, partially melted, granulitic breccias. *Meteor. Planet. Sci.* **39**, 1419–1447.

Connolly H. C., Zipfel J., Grossman J. N., Folco L., Smith C., Jones R. H., Righter K., Zolensky M. and Russell S. S. (2006) The Meteoritical Bulletin 90. *Meteor. Planet. Sci.* **41**, 1383–1418.

Connolly H. C., Smith C., Benedix G., Folco L., Righter K., Zipfel J., Yamaguchi A. and Chennaoui Aoudjehane H. (2007) The Meteoritical Bulletin 93. *Meteor. Planet. Sci.* **43**, 571–632.

Cushing J. A., Taylor G. J., Norman M. D. and Keil K. (1999) The granulitic impactite suite: impact melts and metamorphic breccias of the early lunar crust. *Meteor. Planet. Sci.* **34**, 185–195.

Eberhardt P., Geiss J., Graf H., Grögler N., Krähenbühl U., Schwaller H., Schwarzmüller J. and Stettler A. (1970) Trapped solar wind noble gases, Kr^{81}/Kr exposure ages and K/Ar ages in Apollo 11 lunar material. *Science* **167**, 558–560.

Fernandes V. A., Irving A. J., Kuehner S. M., Gellissen M., Korotev R. L. and Bandfield J. L. (2009) Petrology, bulk composition, Ar–Ar age, and IR emission spectrum of lunar granulite Northwest Africa 4881. *Lunar Planet. Sci.* **40** (abstr. #2009).

Foreman A. B., Korotev R. L., Jolliff B. L. and Zeigler R. A. (2008) Petrography and geochemistry of Dhofar 733: an unusually sodic feldspathic lunar meteorite. *Lunar Planet. Sci.* **34** (abstr. #1853).

Foreman A. B., Korotev R. L., Zeigler R. A., Wittmann A., Kring D. A., Irving A. J. and Kuehner S. M. (2009) Petrographic and geochemical analysis of feldspathic lunar meteorite Shişr 161. *Lunar Planet. Sci.* **40** (abstr. #2304).

Goodrich C.A., Taylor G. J., Keil K., Boynton W. V. and Hill D. H. (1984) Petrology and chemistry of hyperferroan anorthosites and other clasts from lunar meteorite ALHA81005. *Proc. Lunar Planet. Sci. Conf. 15th*, in *J. Geophys. Res.* **89**, C87–C94.

Haskin L. A., Korotev R. L., Rockow K. M. and Jolliff B. L. (1998) The case for an Imbrium origin of the Apollo Th-rich impact-melt breccias. *Meteor. Planet. Sci.* **33**, 959–975.

Hidaka Y., Yamaguchi A. and Ebihara M. (2009) Geochemistry and petrology of meteorite Dhofar 1428. *72nd Annual Meeting Met. Soc.*, #5329 (abstr.).

Hiesinger H. and Head, Jr., J. W. (2006) New views of lunar geoscience: an introduction and overview. In *New Views of the Moon. Reviews in Mineralogy and Geochemistry*, vol. 60 (eds. B. L. Jolliff, M. A. Wieczorek, C. K. Shearer and C. R. Neal). Mineralogical Society of America, Chantilly, Virginia, pp. 1–67.

Hubbard N. J., Rhodes J. M., Wiesmann H., Shih C.-Y. and Bansal B. M. (1974) The chemical definition and interpretation of rock types returned from the non-mare regions of the moon. *Proc. Lunar Sci. Conf.* **5**, 1227–1246.

Hudgins J. A., Spray J. G., Kelley S. P., Korotev R. L. and Sherlock S. C. (2008) A laser probe $^{40}Ar/^{39}Ar$ and INAA investigation of four Apollo granulitic breccias. *Geochim. Cosmochim. Acta* **72**, 5781–5798.

Irving A. J., Kuehner S. M., Korotev R. L., Rumble D. and Hupe G. M. (2006) Mafic granulitic impactite Northwest Africa 3163: a unique meteorite from the deep lunar crust. *Lunar Planet. Sci. Conf.* **37** (abstr. #1365).

Ishii T., Miyamoto M. and Takeda H. (1976) Pyroxene geothermometry and crystallization, subsolidus equilibration temperatures of lunar and achondritic pyroxenes. *Lunar Planet. Sci. Conf.* **7**, 408.

James O. B., Cohen B. A. and Taylor L. A. (2003) Lunar meteorite Dhofar 026: a shocked granulitic breccia, not an impact melt. *Lunar Planet. Sci. Conf.* **34** (abstr. #1149).

Jolliff B. L., Gillis J. J., Haskin L. A., Korotev R. L. and Wieczorek M. A. (2000) Major lunar crustal terranes: surface expressions and crust–mantle origins. *J. Geophys Res.* **105**, 4197–4416.

Jolliff, B. L., Wieczorek, M. A., Shearer, C. K. and Neal, C. R. (eds.) (2006) *New Views of the Moon. Reviews in Mineralogy and Geochemistry volume 60*. Mineralogical Society of America, 772pp.

Jolliff B. L., Rockow K. M., Korotev R. L. and Haskin L. A. (1996) Lithologic distribution and geologic history of the Apollo 17 site: the record in soils and small rock particles from the highlands massifs. *Meteor. Planet. Sci.* **31**, 116–145.

Koeberl C., Warren P. H., Lindstrom M. M., Spettel B. and Fukuoka T. (1989) Preliminary examination of the Yamato-86032 lunar meteorite: II. Major and trace element chemistry. *Proc. NIPR Symp. Antarct. Meteorites* 2, 15–24. Nat. Inst. Polar Res., Tokyo.

Korotev R. L. (1996) On the relationship between the Apollo 16 ancient regolith breccias and feldspathic fragmental breccias, and the composition of the prebasin crust in the Central Highlands of the Moon. *Meteor. Planet. Sci.* **31**, 403–412.

Korotev R. L. (2005) Lunar geochemistry as told by the lunar meteorites. *Chemie de Erde* **65**, 297–346.

Korotev R. L. (2009) Lunar surface geochemistry and lunar meteorites. *Lunar Reconnaissance Orbiter Mission Targeting Meeting* (abstr. #6005).

Korotev R. L. and Irving A. J. (2005) Compositions of three lunar meteorites: Meteorite Hills 01210, Northeast Africa 001, and Northwest Africa 3136. *Lunar Planet. Sci.* **36** (abstr. #1220).

Korotev R. L. and Jolliff B. L. (2001) The curious case of the lunar magnesian granulitic breccias. *Lunar Planet. Sci.* **32** (abstr. #1455).

Korotev R. L., Lindstrom M. M., Lindstrom D. J. and Haskin L. A. (1983) Antarctic meteorite ALHA81005 – not just another lunar anorthositic norite. *Geophys. Res. Lett.* **10**, 829–832.

Korotev R. L., Jolliff B. L., Zeigler R. A., Gillis J. J. and Haskin L. A. (2003) Feldspathic lunar meteorites and their implications

for compositional remote sensing of the lunar surface and the composition of the lunar crust. *Geochim. Cosmochim. Acta* **67**, 4895–4923.

Korotev R. L., Zeigler R. A. and Jolliff B. L. (2006) Feldspathic lunar meteorites Pecora Escarpment 02007 and Dhofar 489: contamination of the surface of the lunar highlands by post-basin impacts. *Geochim. Cosmochim. Acta* **70**, 5935–5956.

Korotev R. L., Zeigler R. A., Jolliff B. L., Irving A. J. and Bunch T. E. (2009) Compositional and lithological diversity among brecciated lunar meteorites of intermediate iron composition. *Meteor. Planet. Sci.* **44**, 1287–1322.

Kuehner S. M., Irving A. J., Gellissen M. and Korotev R. L. (2010) Petrology and composition of lunar troctolitic granulite Northwest Africa 5744: a unique recrystallized magnesian crustal sample. *Lunar Planet. Sci. Conf.* **41** (abstr. #1552).

Laul J. C. and Schmitt R. A. (1973a) Chemical composition of Apollo 15, 16, and 17 samples. *Proc. Lunar Sci. Conf. 4th*, 1349–1367.

Laul J. C. and Schmitt E. A. (1973b) Chemical composition of Luna 20 rocks and soil and Apollo 16 soils. *Geochim. Cosmochim. Acta* **37**, 927–942.

Laul J. C., Wakita H., Showalter D. L., Boynton W. V. and Schmitt R. A. (1972) Bulk, rare earth, and other trace elements in Apollo 14, and 15 and Luna 16 samples. *Proc. Lunar Sci. Conf.* **3**, 1181–1200.

Laul J. C., Hill D. W. and Schmitt R. A. (1974) Chemical studies of Apollo 16 and 17 samples. *Proc. Lunar Sci. Conf.* **5**, 1047–1066.

Lindsley D. (1983) Pyroxene thermometry. *Am. Min.* **68**, 477–493.

Lindstrom M. and Lindstrom D. (1986) Lunar granulites and their precursor anorthositic norites of the early lunar crust. *J. Geophys. Res.* **91**, 263–276.

Lindstrom M. M. and Salpas P. A. (1981) Geochemical studies of rocks from North Ray Crater, Apollo 16. *Proc. Lunar Planet. Sci. Conf.* **12B**, 305–322.

Lindstrom M. M. and Salpas P. A. (1983) Geochemical studies of feldspathic fragmental breccias and the nature of North Ray Crater ejecta. *Proc. Lunar Planet. Sci. Conf.* 13, in *J. Geophys. Res.* **88**, A671–A683.

Lindstrom M. M., Nava D. F., Lindstrom D. J., Winzer S. R., Lum R. K. L., Schuhmann P. J., Schuhmann S. and Philpotts J. A. (1977) Geochemical studies of the white breccia boulders at North Ray Crater, Descartes region of the lunar highlands. *Proc. Lunar Sci. Conf.* **8**, 2137–2151.

LSPET (1973) The Apollo 16 lunar samples: petrographic and chemical description. *Science* **17**, 23–33.

Ma M.-S. and Schmitt R. A. (1982) Chemistry of the matrix, glass coating and an olivine clast from polymict ANT breccia 60035. *Lunar Planet. Sci. Conf.* **8**, 453–454.

Palme H., Baddenhausen H., Blum K., Cendales M., Dreibus G., Hofmeister H., Kruse H., Palme C., Spettel B., Vilcsek E. and Wänke H. (1978) New data on lunar samples and achondrites and a comparison of the least fractionated samples from the earth, the moon, and the eucrite parent body. *Proc. Lunar Planet. Sci. Conf.* **9**, 25–57.

Palme H., Spettel B., Jochum K. P., Dreibus G., Weber H., Weckwerth G., Wänke H., Bischoff A. and Stöffler D. (1991) Lunar highland meteorites and the composition of the lunar crust. *Geochim. Cosmochim. Acta* **55**, 3105–3122.

Papike J. J., Ryder G. and Shearer C. K. (1998) Lunar samples. In *Planetary materials. Reviews in mineralogy*, vol. 36 (ed. J. J. Papike). Mineralogical Society of America, pp. 5-1–5-234.

Ryder G. (1985) *Catalog of Apollo 15 Rocks*, *Part 2. 15306–15468*. JSC 20787, NASA Johnson Space Center, Houston.

Simon S. B., Papike J. J. and Shearer C. K. (1983) Petrology of ALHA81005, the first lunar meteorite. *Geophys. Res. Lett.* **10**, 787–790.

Stöffler D., Bischoff A., Borchardt R., Burghele A., Deutsch A., Jessberger E. K., Ostertag R., Palme H., Spettel B., Reimold W. U., Wacker K. and Wänke H. (1985) Composition and evolution of the lunar crust in the Descartes highlands, Apollo 16. *Proc. Lunar Planet. Sci. Conf.*, in *J. Geophys. Res.* **90**, C449–C506.

Stöffler D., Knöll H.-D., Marvin U. B., Simonds C. H. and Warren P. H. (1980) Recommended classification and nomenclature of lunar highlands rocks – a committee report. In *Proc. Conf. Lunar Highlands Crust* (eds. J. J. Papike and R. B. Merrill). Pergamon Press, pp. 51–70.

Treiman A. H. and Drake M. J. (1983) Origin of lunar meteorite ALHA81005: clues from the presence of terrae clasts and a very low-titanium mare basalt clast. *Geophys. Res. Lett.* **10**, 783–786.

Treiman A. H., Maloy A. K., Shearer, Jr., C. K. and Gross J. (2010) Magnesian anorthositic granulites in lunar meteorites Allan Hills A81005 and Dhofar 309: Geochemistry and global significance. *Meteor. Planet. Sci.* **45**, 163–180.

Warner J. L., Phinney W. C., Bickel C. E. and Simonds C. H. (1977) Feldspathic granulitic impactites and pre-final bombardment lunar evolution. *Proc. Lunar Planet. Sci. Conf.* **8**, 2051–2066.

Wänke H., Palme H., Kruse H., Baddenhausen H., Cendales M., Dreibus G., Hofmeister H., Jagoutz E., Palme C., Spettel B. and Thacker R. (1976) Chemistry of lunar highlands rocks: a refined evaluation of the composition of the primary matter. *Proc. Lunar Sci. Conf.* **7**, 3479–3499.

Warren P. H. (1993) A concise compilation of petrologic information on possibly pristine nonmare Moon rocks. *Am. Min.* **78**, 360–376.

Warren P. H. (1989) KREEP: major-element diversity, trace-element uniformity (almost). In *Workshop on moon in transition: Apollo 14, KREEP, and evolved lunar rocks. LPI Tech. Rpt. 89-03* (eds. G. J. Taylor and P. H. Warren). Lunar and Planetary Institute, Houston, pp. 149–153.

Warren P. H., Jerde E. A. and Kallemeyn G. W. (1990) Pristine Moon rocks: an alkali anorthosite with coarse augite exsolution from plagioclase, a magnesian harzburgite, and other oddities. *Proc. Lunar Planet. Sci. Conf.* **20**, 31–59.

Warren P. H., Ulff-Møller F. and Kallemeyn G. W. (2005) "New" lunar meteorites: Impact melt and regolith breccias and large-scale heterogeneities of the upper lunar crust. *Meteor. Planet. Sci.* **40**, 989–1014.

Wasson J. T., Warren P. H., Kallemeyn G. W., McEwing C. E., Mittlefehldt D. W. and Boynton W. V. (1977) SCCRV, a major component of highlands rocks. *Proc. Lunar Sci. Conf.* **8**, 2237–2252.

Wieler R. (2002) Cosmic-ray-produced noble gases in meteorites. In *Noble gases. Reviews in mineralogy and geochemistry*, vol. 47 (eds. D. P. Porcelli, C. J. Ballentine and R. Weiler). Mineralogical Society of America, Washington, DC, pp. 125–170.

Weisberg M. K., Smith C., Benedix G., Folco L., Righter K., Zipfel J., Yamaguchi A. and Chennaoui Aoudjehane H. (2008) The Meteoritical Bulletin 94. *Meteor. Planet. Sci.* **43**, 1551–1588.

Associate editor: Alan D. Brandon